2026 年研究生国家奖学金个人情况统计表

姓名	刘鸣镭	性别		政治面貌	
学院	古生物学院	专业名称	生物学	学号	
入学时间		身份证号			

项目类别	论文题目或相应名称	刊物名称或审批单位	时间	备注
论文	Terrestrial evidence of the Callovian cooling event from the Middle Jurassic Wanbao Formation, Inner Mongolia, NE China: A Ginkgoites-based perspective	Journal of Palaeogeography	2026 年 5 月	第四作者
科研立项	准噶尔盆地滴南凸起逆断层体系下石炭系火山岩储层裂缝分布规律研究	沈阳师范大学	2026 年 6 月	主持
科研立项	黑龙江嘉荫 K-Pg 界线火山事件地球化学示踪与源区识别	辽宁省教育厅	2025 年 7 月	参与
科研立项	玄武岩储层矿物组成对岩石脆性及裂缝发育定量研究	辽宁省科学技术厅	2025 年 11 月	参与
艺术展演及比赛获奖	第 11 届青年地学论坛	青年地学论坛理事会	2026 年 04 月	作报告

注：1.上述内容应严格按照评选细则如实填写，如发现所填内容与实际不符，将取消评选资格。

2.表格应严格按照填表要求规范填写。

3.备注栏中填写作者（获奖）顺序。

Journal of Palaeogeography, 2026, 15(3): 100351

Available online at www.sciencedirect.com

ScienceDirect

journal homepage: http://www.journals.elsevier.com/journal-of-palaeogeography/

Research article

Terrestrial evidence of the Callovian cooling event from the Middle Jurassic Wanbao Formation, Inner Mongolia, NE China: A *Ginkgoites*-based perspective

Yu-Jin Zhang [a,b], ***Yu-Shuo Liu*** [c,d], ***Chang-Yu Wu*** [c,d], ***Ming-Lei Liu*** [c,d], ***Hong-Wei Ma*** [c,d], ***Miao-Miao Xiang*** [c,d], ***De-Jun Zhang*** [a,b], ***Hai-Hua Zhang*** [a,b], ***Zi-Qing Yu*** [c,d], ***Fan-Hao Gong*** [a,b], ***Fei Liang*** [c,d,*]

[a] *Shenyang Center of Geological Survey, China Geological Survey, Shenyang 110034, Liaoning Province, China*

[b] *Observation and Research Station of Mesozoic Stratigraphic System in Western Liaoning, Ministry of Natural Resources, Shenyang 110034, Liaoning Province, China*

[c] *College of Paleontology, Shenyang Normal University, Shenyang 110034, Liaoning Province, China*

[d] *Key Lab of Evolution of Past Life in Northeast Asia, Ministry of Natural Resources, Shenyang 110034, Liaoning Province, China*

Abstract The Middle Jurassic represents a critical transition from greenhouse to coolhouse conditions, with a cooling episode recorded in the Callovian Stage linked to declining atmospheric CO_2 concentrations (pCO_2) and notable geological activity. However, the relationship between pCO_2 fluctuations and terrestrial evidence remains unclear. Here, we report the first *in situ* zircon U—Pb ages from volcanic interbeds at the coal-bearing Wanbao Formation of the Mangniuhai Coal Mine, Tuquan County, Inner Mongolia, NE China. A weighted-mean age of 163.6±1.2 Ma firmly placed these deposits in the Callovian. Moreover, we present the first quantitative epidermal study of *Ginkgoites longifolius* in this region, focusing on its abaxial stomatal parameters. Stomatal-based paleo-pCO_2 reconstruction yielded a value of 688.5±140.3 ppmv, indicating relatively low pCO_2 value and a cooler climate consistent with previously recognized Callovian cooling phases. Considering the paleogeographic distribution of its habitats, these results suggest that *Ginkgoites longifolius* was adapted to and confined within strongly seasonal temperate–subtropical regimes. These findings are crucial for elucidating the paleoenvironmental context underlying feathered dinosaur diversification and early mammalian evolution during the Callovian.

* Corresponding author. College of Paleontology, Shenyang Normal University, Shenyang 110034, Liaoning Province, China.
E-mail address: liangfei5777@163.com (F. Liang).

Peer review under responsibility of China University of Petroleum (Beijing)

https://doi.org/10.1016/j.jop.2026.100351

Received 18 October 2025; revised 3 December 2025; accepted 14 December 2025; available online 12 March 2026

1. Introduction

Jurassic climates have been largely conceptualized through warm "greenhouse" models characterized by an elevated atmospheric CO_2 concentrations (pCO_2); however, this paradigm is being increasingly contested (Holz, 2015; Li *et al.*, 2022; Judd *et al.*, 2024). The Middle Jurassic (174.1–163.5 Ma) represents a critical transitional interval, with a significant turnover from prevailing warm conditions to cooler climates (Bodin *et al.*, 2020; Li *et al.*, 2022; Judd *et al.*, 2024). Evidence now indicates the intermittent development of "cool mode" or even transient icehouse conditions, often coupled with a demonstrably lower pCO_2, suggesting a far more dynamic and fluctuating climate than previously conceived during the Middle Jurassic (Korte *et al.*, 2015; Alberti et al., 2020; Bodin *et al.*, 2020; Li *et al.*, 2022; Judd *et al.*, 2024; Cavallina *et al.*, 2025). The recognition of these Middle Jurassic "coolhouse" episodes, coexisting with diminished pCO_2 and significant global geological processes (Scotese *et al.*, 2021; Judd *et al.*, 2024), highlights the growing imperative to thoroughly investigate this interval. Examples include the proposed "Callovian Ice Age" linked to pCO_2 drawdown (Dromart *et al.*, 2003), global cooling events potentially triggered by bolide impacts (Scotese *et al.*, 2021), and the demonstrated interplay between pCO_2 variations and global sea level fluctuations (Müller et al., 2008; Bodin *et al.*, 2020).

However, a significant limitation persists, in that our current knowledge of Earth's state during this pivotal period is overwhelmingly constructed from marine proxy archives (Dera *et al.*, 2011; Korte *et al.*, 2015; Alberti et al., 2020), which highlights a critical gap in our understanding as well as an inherent bias in existing paleoclimatic reconstructions. Notably, research focusing on terrestrial records or proxies of the Callovian age remains comparatively sparse, but such records offer unique insights into continental climate dynamics and regional variability, which are often obscured in marine data. Therefore, robust and high-resolution paleoclimatic reconstructions from the continental realm are crucial to achieve a more complete and nuanced understanding of the Middle Jurassic climate change. In addition, the immense potential of continental archives is highlighted by the abundance and diversity of terrestrial vertebrate fauna (Xu *et al.*, 2018; Li *et al.*, 2025), the comprehensive record of major plate tectonic events (Martini and Ortega-Gutierrez, 2018), and evidence of large-scale geological and oceanic events (Dera *et al.*, 2011; Scotese *et al.*, 2021). Moreover, paleobotanical evidence (Wang *et al.*, 2005; Sun et al., 2008, 2018; Yan *et al.*, 2009; Wu *et al.*, 2016; Zhou et al., 2020a; Zhou et al., 2020b; Steinthorsdottir *et al.*, 2022; Huang *et al.*, 2024) serves as an important indicator of past climate change, providing information on temperature, precipitation, and seasonality that complements geochemical proxies and the faunal distribution. Nevertheless, well-preserved terrestrial strata and associated plant fossils from the Callovian with precise age constraints are rare and geographically limited. This scarcity limits the precise determination of the relationships between pCO_2 values and the paleoclimate during this critical interval. Resultantly, we present a quantitative analysis of *Ginkgoites* leaf fossils from the Callovian, providing pivotal fossil evidence for investigating and characterizing the proposed cooling events during this stage.

2. Material and methods

2.1. *Geological setting*

Fossil materials and U–Pb geochronological samples were collected from the Middle Jurassic Wanbao Formation exposed at the Mangniuhai Coal Mine, Tuquan County, Inner Mongolia, China (Fig. 1A). Both the dated tuff samples and plant fossil specimens were obtained from the upper part of the Wanbao Formation (Fig. 1B), which is predominantly composed of mudstone, siltstone, and sandstone, interbedded with thin coal seams and tuff layers. Petrographic observations showed that the dated sample is a rhyolitic tuff with a typical tuffaceous texture, which mainly consists of vitric fragments (~60%) and rhyolitic lithic fragments (~30%), with minor

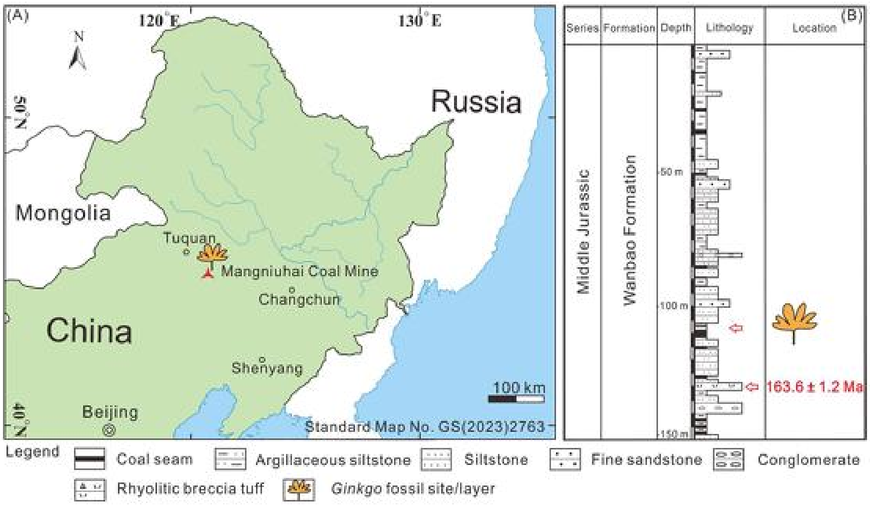

Fig. 1 Fossil site and stratigraphic column of the Wanbao Formation in the Tuquan Basin. **A)** Fossil site of *Ginkgoites longifolius*; **B)** Composite stratigraphic column showing the fossil-bearing layer and tuffaceous siltstone sample location.

Fig. 2 Rhyolitic tuff sample for U—Pb dating. **A)** and **B)** Tuff hand specimen; **C)** and **D)** Zircon U—Pb dating sample with tuff textures in single and crossed polarized light. Cr = Crystal clasts; Lv = Volcanic lithic clasts; Vit = Vitric clasts.

crystal fragments (~10%) dominated by feldspar and quartz. An anorthoclase crystal-rich tuffaceous siltstone sample (Sample No. WB01TW3) was collected from a lens within the coal-bearing strata exposed at the mine outcrop, with a thickness of approximately 20 cm (Fig. 2A). The rock has a pyroclastic texture with a massive structure, predominantly composed of volcanic lithic clasts, vitric clasts, crystal clasts, and volcanic ash (Fig. 2B–D). All components are cemented by volcanic ash (Fig. 2C and D).

2.2. *U—Pb dating*

Petrographic thin sections were prepared and analyzed at the Northeast Mineral Resources Supervision and Testing Center, Ministry of Natural Resources. The rhyolitic tuff texture was examined using an Olympus BX53 polarizing microscope under both plane-polarized and cross-polarized light. Zircon separation, mounting, and cathodoluminescence (CL) imaging were conducted at the laboratory of the Hebei Institute of Regional Geological and Mineral Survey. Zircon grains were recovered using conventional heavy-liquid and magnetic separation techniques, from which euhedral and inclusion-free grains were handpicked under a binocular microscope. The selected zircons were mounted in epoxy resin and polished to expose their internal structures. CL imaging, in combination with transmitted and reflected light microscopy, was used to identify microfractures,

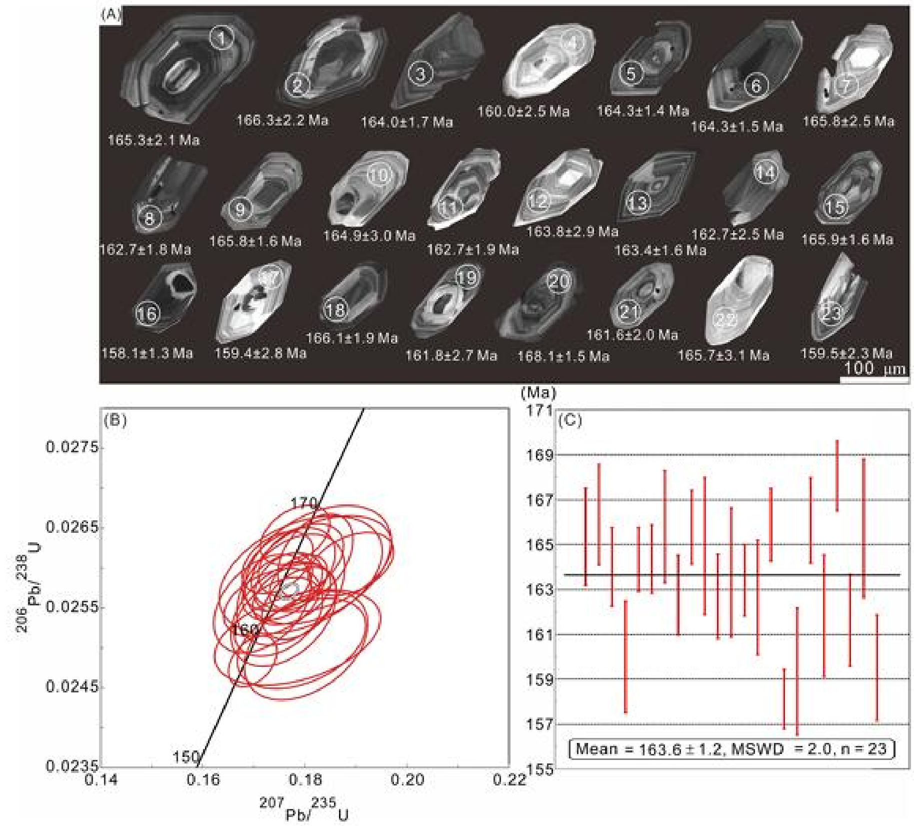

Fig. 3 Illustration of zircon U—Pb dating analysis and results. **A)** CL images of zircons; **B)** Concordia plot of the tuffaceous siltstone sample; **C)** Weighted mean ages of the tuffaceous siltstone sample.

inclusions, oscillatory zoning and other internal features, thereby determining suitable analytical domains.

LA–ICP–MS U—Pb analysis was performed at the Shenyang Center, China Geological Survey, using an Agilent 7900 inductively coupled plasma mass spectrometer coupled to a Photon Machine laser ablation system. Analytical conditions included a laser spot diameter of 35 μm, a repetition rate of 8 Hz, and an energy density of approximately 4.24 $J \cdot cm^{-2}$, with He as the carrier gas. NIST610 glass was used as the external standard and ^{29}Si as the internal standard. For quality control, zircon standards 91500 and Plesovice (Jackson *et al.*, 2004; Geng *et al.*, 2011; Hou *et al.*, 2009) were analyzed, with two analyses of 91500 and one of Plesovice conducted after every eight unknown analyses. Data reduction was carried out using ICPMS-DataCal version 10.9, and concordia diagrams together with weighted mean age calculations were obtained using Isoplot (Ludwig, 2003; Liu *et al.*, 2008).

2.3. *Cuticle treatment*

First, leaf fossils were first photographed using a 3D large depth-of-field microscopy system (Olympus DSX–1000). Next, cuticles were isolated from the rock matrix and treated following the Schulze maceration method (Dilcher, 1974). Cuticle maceration was conducted using an acid—alkali procedure as described by Liang *et al.* (2021) and Liu *et al.* (2025). After maceration, a portion of the cuticle specimen was mounted in glycerin jelly for observation and imaging under an optical microscope (Leica DM3000) and a fluorescence microscope (Leica DM–4B). The remaining specimens were mounted on stubs, coated, and observed using a scanning electron microscope (SEM; HITACHI S–4800 instrument). All laboratory procedures were conducted in the Key Laboratory of Paleontological Evolution in Northeast Asia, Shenyang Normal University, Ministry of Natural Resources. The fossil specimens, prepared microscope slides, and SEM stubs are permanently housed in the College of Paleontology, Shenyang Normal University, Liaoning Province, China. Leaf anatomical terminology follows that of Harris (1974).

2.4. *Statistics*

The stomatal index (SI) was calculated using the following formula: SI (%) = [SD/(SD+ED)]×100, where SD represents the stomatal density (number of stomates per unit area) and ED represents the epidermal cell density (number of epidermal cells per unit area). pCO_2 was primarily reconstructed using two

Table 1 Zircon U—Pb dating results of the tuffaceous siltstone sample.

Spot	Th (ppm)	U (ppm)	Th/U	Isotopic ratios						Isotopic ages (Ma)						Concordance
				$^{207}Pb/^{206}Pb$		$^{207}Pb/^{235}U$		$^{206}Pb/^{238}U$		$^{207}Pb/^{206}Pb$		$^{207}Pb/^{235}U$		$^{206}Pb/^{238}U$		
				Ratio	1σ	Ratio	1σ	Ratio	1σ	Age	1σ	Age	1σ	Age	1σ	
WB01TW3–1	451	321	1.41	0.0494	0.0017	0.1768	0.0060	0.0260	0.0003	168.6	86.1	165.3	5.2	165.3	2.2	99%
WB01TW3–2	155	254	0.61	0.0509	0.0016	0.1820	0.0049	0.0261	0.0004	235.3	72.2	169.8	4.2	166.3	2.2	97%
WB01TW3–3	135	407	0.33	0.0499	0.0017	0.1756	0.0052	0.0258	0.0003	190.8	81.5	164.2	4.5	164.0	1.7	99%
WB01TW3–4	39	86	0.45	0.0529	0.0035	0.1786	0.0107	0.0251	0.0004	324.1	156.5	166.8	9.2	160.0	2.5	95%
WB01TW3–5	205	325	0.63	0.0481	0.0015	0.1787	0.0038	0.0258	0.0002	105.6	72.2	167.0	3.3	164.3	1.4	98%
WB01TW3–6	691	678	1.02	0.0500	0.0014	0.1758	0.0037	0.0258	0.0002	194.5	64.8	164.4	3.2	164.4	1.5	99%
WB01TW3–7	47	96	0.49	0.0484	0.0030	0.1833	0.0091	0.0261	0.0004	120.5	140.7	170.9	7.8	165.8	2.5	96%
WB01TW3–8	204	252	0.81	0.0492	0.0017	0.1735	0.0062	0.0256	0.0003	166.8	81.5	162.5	5.4	162.7	1.8	99%
WB01TW3–9	102	182	0.56	0.0471	0.0023	0.1890	0.0055	0.0260	0.0003	53.8	111.1	175.8	4.7	165.8	1.6	94%
WB01TW3–10	37	76	0.48	0.0485	0.0032	0.1792	0.0105	0.0259	0.0005	124.2	148.1	167.3	9.1	164.9	3.1	98%
WB01TW3–11	124	228	0.55	0.0509	0.0014	0.1788	0.0048	0.0256	0.0003	235.3	63.0	167.1	4.2	162.7	1.9	97%
WB01TW3–12	47	97	0.48	0.0508	0.0022	0.1773	0.0070	0.0257	0.0005	231.6	98.1	165.7	6.0	163.8	2.9	98%
WB01TW3–13	101	217	0.47	0.0488	0.0017	0.1774	0.0050	0.0257	0.0003	139.0	79.6	165.8	4.3	163.4	1.6	98%
WB01TW3–14	57	116	0.49	0.0497	0.0021	0.1717	0.0063	0.0256	0.0004	189.0	96.3	160.9	5.4	162.7	2.6	98%
WB01TW3–15	97	194	0.50	0.0489	0.0013	0.1747	0.0046	0.0261	0.0003	142.7	64.8	163.5	4.0	165.9	1.6	98%
WB01TW3–16	1075	781	1.38	0.0496	0.0010	0.1698	0.0031	0.0248	0.0002	189.0	50.9	159.2	2.7	158.1	1.3	99%
WB01TW3–17	43	94	0.46	0.0530	0.0024	0.1802	0.0080	0.0250	0.0004	331.5	99.1	168.3	6.9	159.4	2.8	94%
WB01TW3–18	460	326	1.41	0.0501	0.0017	0.1792	0.0055	0.0261	0.0003	198.2	77.8	167.4	4.7	166.1	1.9	99%
WB01TW3–19	62	118	0.52	0.0447	0.0030	0.1758	0.0068	0.0254	0.0004	203.2	74.6	164.5	5.9	161.8	2.7	98%
WB01TW3–20	69	186	0.37	0.0493	0.0013	0.1781	0.0045	0.0264	0.0002	161.2	67.6	166.4	3.9	168.1	1.5	99%
WB01TW3–21	142	193	0.74	0.0502	0.0017	0.1748	0.0057	0.0254	0.0003	205.6	79.6	163.6	5.0	161.6	2.0	98%
WB01TW3–22	24	50	0.48	0.0462	0.0032	0.1825	0.0095	0.0260	0.0005	5.7	159.2	170.2	8.1	165.7	3.1	97%
WB01TW3–23	61	87	0.70	0.0503	0.0027	0.1793	0.0083	0.0251	0.0004	209.3	122.2	167.5	7.2	159.5	2.3	95%

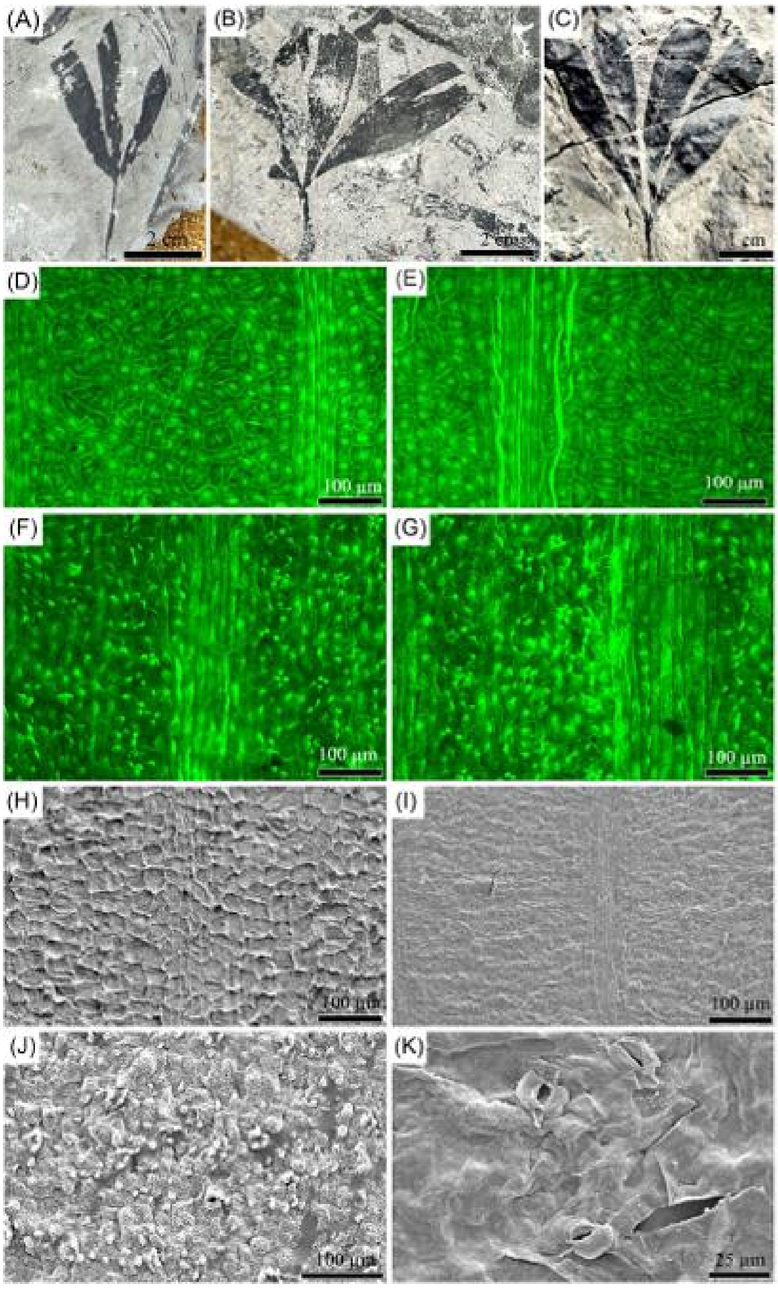
(A)
2 cm
(B)
(C)
1 cm
(D)
100 μm
(E)
100 μm
(F)
100 μm
(G)
100 μm
(H)
100 μm
(I)
100 μm
(J)
100 μm
(K)
25 μm

established methods: the Nearest Living Relative (NLR) approach (McElwain and Chaloner, 1995, 1996; McElwain and Steinthorsdottir, 2017) and the Barclay SI-pCO_2 curve (Barclay and Wing, 2016). The NLR method incorporated two standardization criteria: Carboniferous (CS) and Recent (RS). Reconstructed pCO_2 values were validated via comparison with established global geochemical models and previously reported stomatal index-based CO_2 concentration data. Imaging was performed using fluorescence microscopy with a grid of 0.09 mm^2 (0.3 mm×0.3 mm). The following formulae were employed:

$$\text{Carboniferous standardization: } pCO_2 = SI_{NLE}/SI_{Fossil} \times 2pCO_{2NLE} \quad (1)$$

$$\text{Recent standardization: } pCO_2 = SI_{NLE}/SI_{Fossil} \times 1.2pCO_{2NLE} \quad (2)$$

$$\text{Barclay SI–}pCO_2\text{ curve: } pCO_2 = 9920.9\,(SI)^{-1.484} \quad (3)$$

among, pCO_{2NLE} = 300 ppmv; NLE means "nearest living equivalents"; $SI_{NLE} = SI_{Ginkgo\ biloba}$ which was a fixed value of 12.1 (Beerling and Royer, 2002; McElwain and Steinthorsdottir, 2017).

3. Results

3.1. *Zircon U—Pb dating*

Fig. 3A illustrates the representative cathodoluminescence (CL) images of zircon grains, selected LA-ICP-MS analytical spots, and corresponding ages; concordia diagrams and weighted mean age plots are presented in Fig. 3B and C. Detailed analytical results, including U and Th contents, isotopic ratios, and individual grain ages, are given in Table 1.

A total of 28 analyses of 28 zircon grains were conducted, of which 23 grains exhibited <10% discordance. These 23 analyses yielded $^{206}Pb/^{238}U$ ages (for grains younger than 1.0 Ga) ranging from 168.1 Ma to 158.1 Ma, displaying a relatively narrow distribution. The zircons were predominantly sub-euhedral to euhedral, with grain lengths ranging from 100 μm to 300 μm and aspect ratios of 1—3. They displayed well-developed oscillatory zoning in CL images (Fig. 3A) and had Th/U ratios between 0.33 and 1.41, consistent with a magmatic origin (Koschek, 1993).

Petrographic and geochronological characteristics showed that the sample was derived from a rhyolitic tuff. All concordant data plotted on or near the concordia curve yielded a weighted mean $^{206}Pb/^{238}U$ age of 163.6±1.2 Ma (n = 23, MSWD = 2.0; Fig. 3B and C). This age was interpreted as representing the timing of the volcanic eruption that produced the rhyolitic tuff.

3.2. *Systematic paleontology*

Order Ginkgoales Gorozhankin
Family Ginkgoaceae Engler
Genus *Ginkgoites* Seward, 1919
Ginkgoites longifolius (Phillips) Harris, 1946

1829. *Sphenopteris longifolia* Phillips, p. 148; pl. 7, fig. 17 (Holotype) *.

1900. *Baiera phillipsi* Nathorst: Seward, p. 269; pl. 9, fig. 4; text-fig. 47.

1936. *Ginkgoites phillipsi* (Nathorst) Florin, p. 107.

1944. *Baiera canaliculata* Harris, p. 680; text-figs. 6b, 6c, 7, 8.

1946. *Ginkgoites longifolius* (Phillips) Harris, p. 20; text-figs. 6, 7.

1974. *Ginkgo longifolius* (Phillips) Harris: Harris *et al.*, p. 21; text-figs. 6—8.

Specimens examined: MN-07A, MN-07B, MN-09, MN-016, MN-023, MN-054, MN-065, MN-076, TQG-01, TQG-02, TQG-04, TQG-05, TQG-06, TQG-010, TQG-011, TQG-035

Locality and horizon: Tuquan County, Inner Mongolia, Northeast China.

Stratigraphy and age: Wanbao Formation, Callovian

Diagnosis: Leaf petiolate; lamina deeply divided into 4–8 primary segments, each segment simple or occasionally forked, producing up to 16 ultimate lobes. Lamina base with a basal angle typically around 90° (commonly 60°—120°). Lobes approximately 10 mm wide, with apices rounded to subacute. Venation more or less distinct, with 5—10 primary veins per lobe, arising by repeated dichotomy from the lamina base and slightly converging towards the apex.

Fig. 4 Leaf and epidermal morphology of *Ginkgoites longifolius* from the Middle Jurassic Wanbao Formation in Tuquan, Inner Mongolia. **A–C)** Leaf and petiole morphology; specimen numbers: MN-07A, MN-09, and TQG-01; **D–E)** Adaxial epidermis under fluorescence microscope; showing cell morphologies in vein and inter vein areas; slide number: TQG-01-001; **F–G)** Abaxial epidermis under fluorescence microscope; showing cell morphologies in vein and inter vein areas, and papillae; slide number: TQG-01-001; **H)** Inner surface of the adaxial epidermis under SEM; SEM number: TQG-04-001; **I)** Outer surface of the adaxial epidermis under SEM; SEM number: TQG-02-001; **J)** Outer surface of the abaxial epidermis under SEM showing stomata with strong papillae; SEM number: TQG-05-002; **K)** Inner surface of the abaxial epidermis under SEM; the guard cells are reniform with subsidiary cells, SEM number: TQG-06-001.

Epidermis hypostomatic. Stomata irregularly distributed, predominantly longitudinally oriented; guard cells reniform, surrounded by 5–7 slightly depressed subsidiary cells. Papillae well-developed and robust, occurring on the outer surfaces of periclinal walls of abaxial epidermal cells; papillae on subsidiary cells overarching and partially covering the stomatal pits. Trichomes absent.

Description: The fan-shaped lamina has petioles that are approximately 20 mm in length (Fig. 4A–C). The lamina is deeply divided into 4–8 primary segments, with a basal angle typically around 90° (commonly 60°–120°), measuring 60–70 mm in length and 40–80 mm in width (Fig. 4A–C). Each segment is typically bifurcated distally, forming two lobes, and individual lobes have 5–10 veins (Fig. 4B and C). The epidermis is hypostomatic. Vein areas are composed of indistinctly narrower and slightly elongated cells (Fig. 4D–G). In the adaxial (upper) cuticle, cells between veins are predominantly isodiametric and polygonal in shape, becoming somewhat elongated adjacent to the vein margins in the inner-surface view. The anticlinal walls are straight (Fig. 4D, E, H). The outer periclinal walls of adaxial epidermal cells are flat in the outer-surface view (Fig. 4I). The abaxial (lower) cuticle has distinctly differentiated vein regions of approximately 150 μm wide and interveinal regions of approximately 300 μm wide (Fig. 4F and G). Cells along the vein areas are narrower and more or less elongated, often with conspicuous longitudinal walls; interveinal cells are typically isodiametric, polygonal, and aligned in short rows (Fig. 4F and G). The outer periclinal walls of ordinary abaxial epidermal cells are occasionally thickened, bearing solid or hollow papillae, and trichomes are absent (Fig. 4F, G, J). Stomata are scattered in interveinal areas and occasionally in short rows, with a variable orientation but are most commonly aligned longitudinally (Fig. 4F, G, H, J, K). Guard cells are slightly sunken, partially covered by the papillae of subsidiary cells (Fig. 4H–K). Subsidiary cells are thickened, forming a rim around the stomatal pit, and each cell also bears solid or hollow papillae. Trichomes are absent (Fig. 4H–J).

Comparison: The fossil genus *Ginkgoites* encompasses leaf fossils morphologically similar to *Ginkgo biloba*, but lack definitive evidence (e.g., reproductive organs attached to leaves) to classify them as such (Seward, 1919; Florin, 1936). The validity and application of *Ginkgoites* have been debated, with differing viewpoints emerging over time (Florin, 1936; Tralau, 1968; Harris, 1974; Zhou et al., 2020b). Some researchers have argued for its abandonment, considering it either a junior synonym or subsuming it within the Ginkgoaceae (Tralau, 1968; Harris, 1974). Conversely, others have maintained *Ginkgoites* as a distinct genus, re-evaluating its diagnostic characteristics to preserve its original definition (Seward, 1919; Krassilov, 1972; Watson *et al.*, 1999). Given the pragmatic advantages of *Ginkgoites*, particularly in its ease of use and differentiation from other ginkgoalean fossils (Zhou et al., 2020b; Liu *et al.*, 2025), we advocate for its continued recognition to promote taxonomic consistency and straightforward fossil identification. The morphology of *Ginkgoites longifolius* leaves is typically characterized by their long petioles, 90° basal angle, and 4–8 deeply lobed segments. Their cuticles possess hypostomatic stomata and straight anticlinal walls. These features distinguish them from other *Ginkgoites* species. *Ginkgoites huttoni* and *G. sibirica* include a few similar leaves that match *G. longifolius* in form, but they can be distinguished by their leaf width and cuticle anatomy. *Ginkgoites huttoni* has trichomes, and *G. sibirica* is distinguished by its lack of hollow papillae on the subsidiary cells. Table 2 lists more detailed comparisons with similar species. Based on the external shape and cuticle features, the present fossil leaves align with *Ginkgoites longifolius*, suggesting they should be assigned to the same species.

3.3. Paleoclimatic reconstruction

In this study, 25 square areas of 0.09 mm^2 were selected from the lower epidermal cuticle of *Ginkgoites longifolius* (Supplementary Table S1). The estimated pCO_2 values derived from the Barclay and Wing model showed an average of 688.54 ± 140.33 ppmv, whereas the McElwain model (RS) yielded an average of 718.51 ± 99.07 ppmv. These data are presented in Fig. 5.

4. Discussion

4.1. Age of the Wanbao Formation in Tuquan County

The fossil flora of the Wanbao Formation in the Tuquan region (southern sector of the Greater Khingan Range) is characterized by a *Coniopteris–Phoenicopsis–Raphaelia* assemblage (Zhang et al., 2018a, 2019). Quantitative analysis of the macrofloral composition revealed a dominance of ferns (Filicopsida, 26.9%) and ginkgoaleans (Ginkgoales, 38.5%) and a substantial proportion of conifers

Table 2 Comparisons with similar species with *Ginkgoites longifolius* of the Middle Jurassic.

Species	Leaf shape	Lamina length (cm)	Lamina width (cm)	Lobes number	Vein density	Cuticle			Reference
						Type	Anticlinal wall	Guard cells	
Ginkgoites longifolius	Fan-shaped Base angle: 90°	6–7	4–8	4–16	5–10/lobe	Hypostomatous	Straight	Sunken	This paper
G. huttonii	Fan-shaped Base angle: 90°–120°	3–5	Unknown	4–6	25/cm	Amphistomatous	Unknown	Sunken	Zhou et al. (2020b)
G. obrutschewii	Cuneate to broadly cuneate	2–5	0.8–1.8	4	9–11/cm	Hypostomatous	Curved	Unknown	Seward (1919)
G. qaidamensis	Cuneate to fan-shaped Base angle: 70°–110°	5–8	Unknown	4–6	12/cm	Amphistomatous	Straight or slightly curved	Slightly sunken	Li *et al.* (1988)
G. shiguaiensis	Semicircular to fan-shaped Base angle: 80°–220°	3–4	6–7	4	9–12/5 mm	Amphistomatous	Curved	Unknown	Sun *et al.* (2008)
G. sibirica	Fan-shaped to semicircular Base angle: 150°–180°	6–7.5	10–13	8–10 or 12–14, rarely 6–8	3–8/lobe	Hypostomatous	Straight or slightly curved	Slightly sunken	Zhou et al. (2020b)
G. taeniatus	Fan-shaped to broadly fan-shaped Base angle: 60°–90°	Unknown	Unknown	4–8	4–8/lobe	Unknown	Unknown	Unknown	Zhou et al. (2020b)
G. taochuanensis	Narrowly fan-shaped base angle: 50°	3	Unknown	6	6/lobe	Amphistomatous	Straight or slightly curved	Sunken	Zhou et al. (2020b)
G. yaojiensis	Semicircular Base angle: 180°	2.5–3	4–5.5	6–8	13/lobe	Hypostomatous	Slightly curved	Unknown	Zhou et al. (2020b)
Ginkgo daohugouensis	Base angle: 110–140°	Unknown	Unknown	4 or 6	12–14/cm	Hypostomatous	Straight	Unknown	Sun *et al.* (2018)
G.parvifolia	Base angle: 130°	Unknown	Unknown	6	5–7/lobe	Amphistomatous	Straight to slightly curved	Sunken	Sun *et al.* (2018)
G.cuneifolia	Base angle: About 45°	Unknown	Unknown	4	18/cm	Amphistomatous	Straight	Unknown	Sun *et al.* (2018)

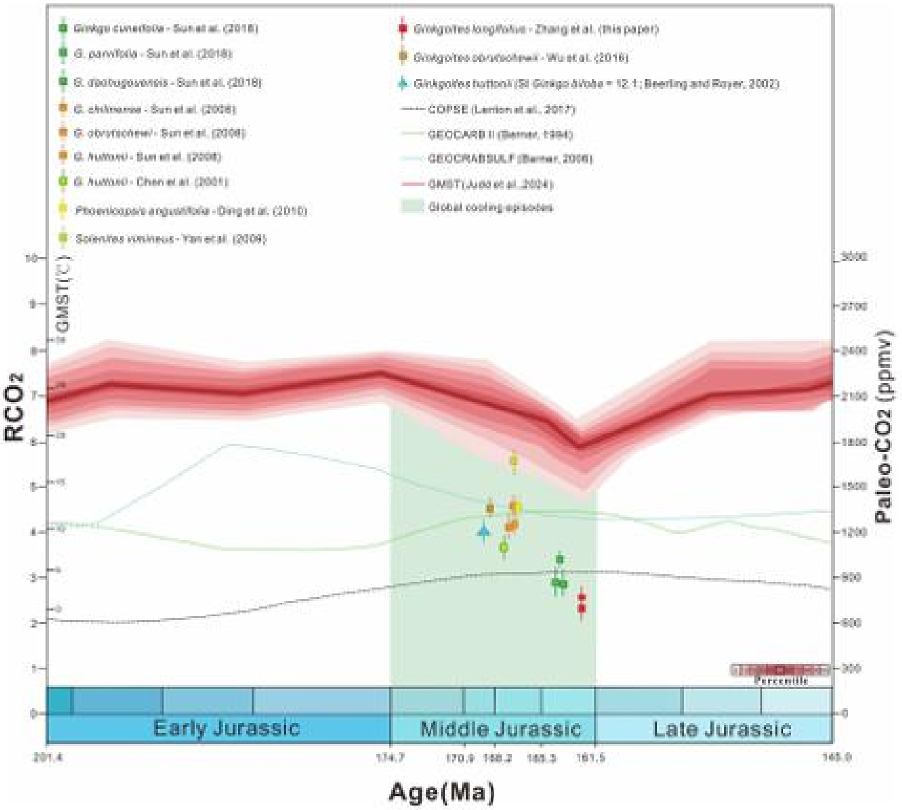

Fig. 5 Estimates of the Middle Jurassic pCO_2 values determined in this study and previously published reports. Curves and data represent geochemical models (GEOCARB II, Berner, 1994; GEOCARB III, Berner and Kothavala, 2001; GEOCARBSULF, Berner, 2006; COPSE, Lenton *et al.*, 2017; and GMST, Judd *et al.*, 2024) and some semi-quantitative paleo-pCO_2 estimates from the Middle Jurassic based on fossil plants (Chen et al., 2001; Beerling and Royer, 2002; Sun et al., 2008, 2018; Yan et al., 2009; Ding et al., 2010; Wu et al., 2016) using the SR method.

(Coniferales, 19.2%). Minor components included horsetails (Equisetales, 7.7%), cycads (Cycadales, 3.8%), and gymnosperm reproductive organs, such as pollen, cones, and seeds, which comprised 3.8% of the assemblage (Yang, 1985; Zhang *et al.*, 2019). In both taxonomic composition and relative abundance, the Wanbao flora exhibited close affinities with several well-documented Middle Jurassic floras, including: the Haifanggou Formation flora of Beipiao, Liaoning (Mi *et al.*, 1996), the Baiyanghe flora of the Junggar Basin, Xinjiang (Sun *et al.*, 2021), and the Xishan flora of Beijing (Chen *et al.*, 1984). These affinities indicate that the Wanbao flora of the Tuquan Basin is coeval with and, therefore, belongs to the Middle Jurassic.

The coal-bearing strata of the Wanbao Formation in the Tuquan Basin have long lacked high-precision ages. Detrital-zircon U–Pb dates obtained by LA-ICP-MS have a broad interval (1221–171 Ma) with large uncertainties (Wang *et al.*, 2013; Yu, 2022), hampering the development of a reliable regional chronostratigraphic framework and poorly constraining the age of the fossil-bearing horizons. Recent advances in zircon U–Pb geochronology have made radiometric dating of volcanic tuffs a powerful tool for stratigraphic division and correlation (Zhang et al., 2018b; MacLennan *et al.*, 2024; Zou *et al.*, 2024). In the Longjiang section on the eastern side of the middle segment of the Greater Khingan Range, tuffs interbedded with the lower and upper parts of the coal-bearing sequence have ages of 165.2±1.7 and 162.1±1.6 Ma, respectively, corresponding to the late Middle Jurassic (Callovian). Notably, numerous tuff layers are distributed throughout the Tuquan Basin, providing stable marker horizons for inter-basin correlations.

To the best of our knowledge, the present study, is the first to report a high-precision zircon U—Pb age from a volcanic tuff intercalated within the Wanbao Formation in the central—southern Greater Khingan Range. The tuff yields an age of 163.6±1.2 Ma, assigning the fossil-bearing strata to the Callovian Stage of the Middle Jurassic. This new radiometric constraint substantiates the age inferred from paleofloral correlations and provides a firm chronostratigraphic anchor for the coal-bearing succession. Consequently, the accuracy of regional stratigraphic correlations is enhanced, underpinning the construction of an accurate chronostratigraphic framework for the basin to reconstruct the geological evolution of the Tuquan Basin and adjacent areas.

4.2. Paleogeography and paleoclimate of the Middle Jurassic Callovian

The Jurassic is widely regarded as a greenhouse interval, with atmospheric CO_2 levels being substantially higher than those observed today (Berner, 1994). Global near-surface and sea-surface temperatures were elevated by 5—10 °C compared to the present (Sellwood et al., 2008). However, evidence has shown that there was significant climatic variability within the Jurassic, including alternating warm and cool intervals (Price et al., 2009; Dera *et al.*, 2011; Korte et al., 2011; Huang *et al.*, 2024; Cavallina *et al.*, 2025). Marine $\delta^{18}O$ records have identified high-temperature intervals in the Toarcian and Oxfordian–Kimmeridgian (Dera *et al.*, 2011), but other proxies indicate transient cooling episodes in the Pliensbachian and early Bajocian (Korte et al., 2011; Bodin *et al.*, 2020). In the Northern Hemisphere, biostratigraphic and geochemical data have indicated short cold pulses in the Callovian (Dromart *et al.*, 2003). As shown in Fig. 5, both calculated pCO_2 ranges fall well within the established confidence intervals, indicating reasonable model agreement with global mean surface temperature (GMST) reconstruction curves (Judd *et al.*, 2024). Compared to contemporaneous data spanning the Middle Jurassic, the pCO_2 values obtained for the Callovian Stage in the present study demonstrate a notable decrease. This reduction aligns temporally with the recognized Callovian cooling event (often termed the "Callovian Ice Age"), which has been hypothesized to be linked to bolide impact events (Dromart *et al.*, 2003; Scotese *et al.*, 2021). The fluctuations observed in our stomatal-based pCO_2 estimates (as shown in Fig. 5) were effectively correlated with independent proxy curves, specifically those derived from GMST reconstruction (Judd *et al.*, 2024). *Ginkgo*-based stomatal proxies for reconstructing past atmospheric pCO_2 concentrations were reliable and effective (Zhou et al., 2020a; Zhou et al., 2020b; Steinthorsdottir *et al.*, 2022); however, prior studies have estimated that climate variables such as temperature, precipitation, and seasonality, have no significant influence during the Early Jurassic (Steinthorsdottir *et al.*, 2022).

Terrestrial evidence corroborates these marine signals. Plant remains, including *Coniopteris* and *Phoenicopsis*, and changes in floristic composition reflect cooler and more humid intervals in some regions (Oh *et al.*, 2015; Tian *et al.*, 2015; Philippe *et al.*, 2017). Quantitative paleo-pCO_2 reconstruction based on plant cuticles and stomatal parameters has proven effective for constraining atmospheric composition and climate (Retallack, 2001; Royer, 2003; Martínez *et al.*, 2018; Zhou et al., 2020a), but applications remain comparatively sparse in Jurassic deposits. The Yanliao Biota of northeastern China, which comprise successive fossil assemblages from the Beipiao through Linglongta intervals, documents temporal changes in terrestrial ecosystems, indicating climatic shifts from relatively warm/arid to cooler conditions and vice-versa (Huang et al., 2015; Xu *et al.*, 2016; Li *et al.*, 2021). However, most regional studies are qualitative; quantitative stomatal or cuticular reconstructions are needed to better constrain paleo-pCO_2 and terrestrial climate dynamics in the Middle Jurassic.

In the southern Greater Khingan Mountains, paleobotanical data (e.g., *Xenoxylon*, and *Protocedroxylon*) and paleoecological indicators have suggested a cooling signal around the Callovian (Zhang et al., 2021a; Zhang et al., 2021b). Biotic assemblages preserved in the Tiaojishan Formation (e.g., *Anchiornis*, early mammals) dated to ~165 Ma provide additional context for the responses of fauna to the climate during the Middle Jurassic (Hu *et al.*, 2009; Zhou *et al.*, 2019; Li *et al.*, 2025). Therefore, reconstructing the Middle Jurassic climate is essential to interpret the selective pressures influencing the origin and functional diversification of early feathered, small-bodied mammals, and associated terrestrial ecosystems.

During the Early to Middle Mesozoic, the supercontinent Pangaea progressively disintegrated, leading to the global reorganization of paleogeographic patterns and ultimately a split into Laurasia and Gondwana (Holz, 2015). By the late Middle Jurassic, the initial opening of the North Atlantic caused the gradual separation of Eurasia from North America, this tectonic process reshaped the spatial configuration of continental blocks and reorganized paleo-oceanic circulation and the climate regimes it governed (Jenkyns *et al.*, 2002; Dera *et al.*, 2011, 2015). The combined effects of oceanic gateway reconfiguration and continental drift drove latitudinal shifts in climatic zones, influencing regional paleoenvironmental evolution and triggering global-scale climatic events. Overall, the global climate of the Middle Jurassic exhibited latitudinal zonation, with arid, tropical, subtropical, temperate, and cold environments distributed successively from the equator to the poles (Fig. 6; Boucot *et al.*, 2013). This zonal pattern was controlled by latitude as well as by the integrated effects of oceanic circulation, land–sea distribution, and atmospheric circulation, resulting in greater regional climatic complexity.

Ginkgoites longifolius held significant paleogeographic and paleoclimatic implications during the Middle Jurassic, with its distribution largely restricted to subtropical to temperate regions of the mid to high-latitude Laurasian continent in the Northern Hemisphere (Fig. 6). The global spatiotemporal distribution sites of *G. longifolius* are listed in Supplement Table S2. Floristically, this taxon was concentrated in the transitional zone between the Siberian and Eurasiatic–Central provinces (Sun et al., 2015; Li *et al.*, 2024), with fossil records extending from northeastern China to Yorkshire, United Kingdom. This distribution pattern demonstrates the strong ecological adaptation to temperate–subtropical climates. Notably, the absence of *G. longifolius* in lower latitudes may be closely linked to the opening of the Viking Corridor during the late Early Jurassic (Ziegler, 1988; Doré, 1991; Scott and Turton, 2001; Li *et al.*, 2024) and the subsequent rifting and expansion of the North Atlantic (Steiner *et al.*, 1998; Golonka, 2004; Labails *et al.*, 2010). The tectonic and paleogeographic shifts during the Middle Jurassic significantly reconfigured continental layouts and oceanic circulation systems. It is likely that these profound changes intensified aridity and elevated temperatures in low-latitude regions, impeding the southward migration of *G. longifolius* into the tropics. Consequently, the biogeographic distribution of *G. longifolius* was largely confined to the mid to high latitudes of the Laurasian continent in the Northern Hemisphere during the Middle Jurassic. This distribution suggests adaptation to climatic regimes characterized by seasonal transitions between temperate

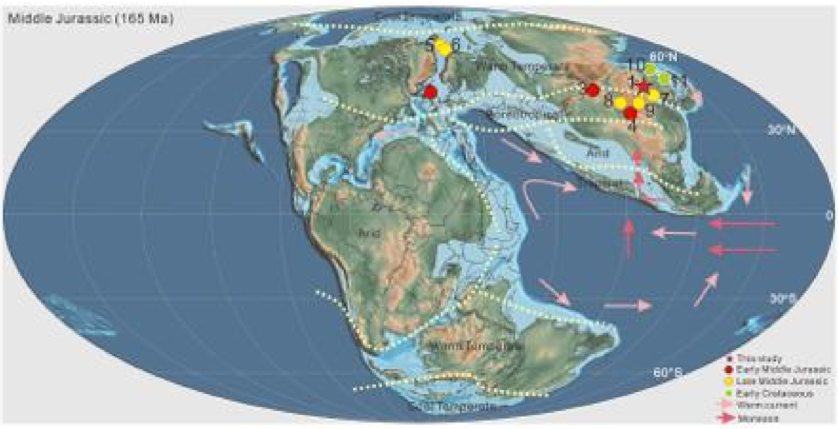

Fig. 6 Paleogeographic distribution of *Ginkgoites longifolius* during the Middle Jurassic Callovian. Detailed site information is given in Supplement Table S2.

and subtropical conditions. The success of *G. longifolius* in these mid to high latitude zones established the climatic foundation for the adaptation of its modern descendant, *Ginkgo biloba*, to extant temperate climates.

Cuticle data from *Ginkgoites longifolius* from the Callovian (~163 Ma) reveals an atmospheric CO_2 concentration of approximately 688.54±140.33 ppmv, a value that is notably lower than that recorded for the Aalenian–Bajocian and Oxfordian–Kimmeridgian stages (Fig. 5), thus suggesting a global cooling event during the Callovian. This cooling event occurred during a relative quiescent interval of global volcanism, when pCO_2 was comparatively low and greenhouse forcing from volcanic activity was significantly weakened. In contrast, the Early Jurassic was influenced by the Karoo–Ferrar Large Igneous Province, which sustained global warming for several million years (Pálfy, 2000; Svensen et al., 2012). During the Middle Jurassic, climatic conditions were relatively stable, with extensive coal deposits developing across the Northern Hemisphere (Johnson *et al.*, 1989; Dong and Sun, 2011; Kostina and Herman, 2013). By the Late Jurassic (Oxfordian–Tithonian), volcanic activity along the circum-Pacific subduction zones reached a peak (Maruyama et al., 1997; Seton et al., 2012), and was accompanied by large-scale volcanism and granitic intrusions in eastern China (Xu *et al.*, 2013; Zhang *et al.*, 2020). Overall, this suggests the low pCO_2 and cooling observed during the Callovian were globally consistent and closely linked to variations in volcanic intensity.

Paleogeographic reconstruction shows that Pangaea's breakup initiated the North Atlantic opening, altering equatorial ocean circulation, weakening poleward heat transport, and progressively isolating the Arctic Ocean, thus intensifying high-latitude cooling (Smith *et al.*, 2004; Korte *et al.*, 2015). The large Puchezh–Katunki impact event in Russia during the Bathonian (~167 Ma) could have also contributed to short-term global cooling (Park and Royer, 2011; Scotese *et al.*, 2021), inducing transient cold pulses in an overall warm background. Dromart *et al.* (2003) proposed the potential existence of small high-latitude ice sheets during the Middle Jurassic, and their albedo effect could have amplified cooling. More recently, pronounced Milankovitch cyclicity (e.g., the 173 kyr short eccentricity cycle) in late Middle Jurassic records from the Croatian carbonate platform has provided new evidence for moderate high-latitude ice sheets (Husinec et al., 2023). In summary, the Callovian cooling event was a multifactorial phenomenon driven by the synergistic effects of plate tectonics, oceanographic reorganization, volcanic activity fluctuations, and astronomical forcing, reflecting the complex coupling in Earth's systems.

4.3. Significance of the Callovian cooling event

The Callovian Stage of the Middle Jurassic (ca. 165–161 Ma) represents a pivotal event in Earth's climatic evolution and has increasingly attracted scientific attention (Dromart *et al.*, 2003; Carmeille *et al.*, 2018). This study, to the best of our knowledge, provides the first direct empirical evidence for a Callovian cooling event based on cuticular evidence from ginkgoalean plants preserved in continental deposits (~163 Ma). Our findings present novel constraints on pCO_2 levels and their associated climatic implications, demonstrating considerable significance for advancing our understanding of global ecosystem patterns and biological evolution. First, the Callovian cooling event marked a pronounced fluctuation in the generally warm Middle Jurassic climate (Dromart *et al.*, 2003; Nunn *et al.*, 2009; Pellenard *et al.*, 2014; Carmeille *et al.*, 2018), demonstrating that Mesozoic greenhouse climates were not permanently stable but rather characterized by alternating warm and cool phases — an important case study for long-term climate change drivers. Second, marine ecosystem records revealed a global temperature decrease of 3–5 °C, with a more pronounced cooling of 5–8 °C in the North Atlantic and Arctic regions (Dromart *et al.*, 2003; Dera *et al.*, 2011). This cooling induced significant ecological responses, including declines in ammonite diversity and their migration into warmer waters (Dromart *et al.*, 2003). Furthermore, pelagic organisms, such as belemnites and benthic taxa such as oysters and *Gryphaea* exhibited $\delta^{18}O$ values that indicated an up to 5 °C cooling amplitude during the Callovian (Price *et al.*, 2023). Collectively, these findings highlight Callovian cooling as a climatic turning point and a direct driver reshaping marine ecosystem structure and function, with profound implications for biological evolution during the Middle Jurassic.

Terrestrial ecosystem records also reveal the impacts of the Callovian cooling event. Palynological analyses have shown that in the Haifanggou Formation of Chaoyang, western Liaoning, and the Wanbao Formation in the Longjang Basin, western Heilongjiang, the proportion of ferns (e.g., *Cladophlebis*) decreased markedly from approximately 60% to about 30% (Pu and Wu, 1985; Zhang et al., 2021a). Conifers and cycads progressively replaced ferns to become the dominant plant groups. The vegetation pattern shifted from a warm-adapted cycad–bennettitalean association to a more cold-tolerant coniferous forest, reflecting a regional climatic transition from warm to cool conditions (Zhang et al., 2018b). The pedogenic and sedimentological characteristics of contemporaneous paleosols in the Sichuan Basin further corroborate this climatic cooling trend (Li *et al.*, 2022). The Callovian cooling event temporally and spatially coincides with the concentrated occurrence of feathered dinosaur fossils, such as those from the Jehol Biota, suggesting that this climatic shift played a pivotal role in the early evolution of feathers. For example, numerous exquisitely preserved feathered dinosaur fossils have been discovered in volcanic ash deposits from the Daohugou area of Ningcheng, Inner Mongolia, and the Jianchang area of western Liaoning (Hu *et al.*, 2009), with dated to the Callovian. This close temporal and spatial correspondence indicates a potential causal relationship between the onset of feather evolution and climatic cooling. Furthermore, lower temperatures would have increased the selective pressure for insulating plumage and simultaneously promoted the functional diversification of feathers toward aerodynamic roles. In the Daohugou Biota, taxa such as *Epidendrosaurus ningchengensis* and *Pedopenna daohugouensis* already exhibited an incipient differentiation between downy feathers (for thermoregulation) and pennaceous feathers (for aerodynamic purposes) (Longrich *et al.*, 2012; Xu and Barrett, 2025). This pattern reflects the combined effects of climatic stress, ecological adaptations, and thermoregulatory demands, which may have provided the key driving forces for the multifunctional evolution of feathers.

5. Conclusions

1) This study reports a high-precision LA–ICP–MS zircon U—Pb age of 163.6±1.2 Ma from a rhyolitic tuff intercalated in the Middle Jurassic Wanbao Formation of Tuquan County for the first time, firmly assigning its deposition to the Callovian Stage.
2) Morphological analysis of *Ginkgoites longifolius* leaves from the Callovian yielded a quantitative pCO_2 estimate (688.54±140.33 ppmv), providing crucial paleoenvironmental context for understanding concurrent global cooling events, feathered dinosaur diversification, and early mammalian evolution.
3) The confinement of *Ginkgoites longifolius* to Laurasian mid- to high-latitudes during the Middle Jurassic reflects paleogeographic and climatic constraints, indicating adaptation to seasonal temperate to subtropical regimes and offering a biogeographic framework relevant to the climatic affinities of its extant descendant, *Ginkgo biloba*.

CRediT authorship contribution statement

Yu-Jin Zhang: Writing — original draft, Resources, Methodology, Funding acquisition. **Yu-Shuo Liu:** Methodology, Investigation, Data curation. **Chang-Yu Wu:** Methodology, Investigation, Formal analysis, Data curation. **Ming-Lei Liu:** Writing — original draft, Methodology, Investigation, Formal analysis, Data curation. **Hong-Wei Ma:** Methodology, Investigation. **Miao-Miao Xiang:** Methodology, Investigation. **De-Jun Zhang:** Resources, Methodology, Funding acquisition, Data curation. **Hai-Hua Zhang:** Resources, Data curation, Conceptualization. **Zi-Qing Yu:** Methodology, Investigation. **Fan-Hao Gong:** Investigation, Funding acquisition, Conceptualization. **Fei Liang:** Writing — review & editing, Writing — original draft, Supervision, Methodology, Funding acquisition, Data curation, Conceptualization.

Conflicts of interest

The authors declare that they have no conflict of interest.

Acknowledgements

The authors acknowledge the support of the National Natural Science Foundation of China (Grant Nos. 42172024, 42172017, 92479206), and China Geological Survey Projects (Grant Nos. DD202402079, DD20230220), and the Fundamental Research Funds for the Liaoning Province (No. 2024—MSLH—496). Thanks are also extended to our colleagues T. Yang and Y.G. Yang for their helps in the field work for fossil collecting, and to the editor and anonymous reviewers for their kind comments on the manuscript.

References

Alberti, M., Leshno, Y., Fürsich, F.T., Edelman-Furstenberg, Y., Andersen, N., Garbe-Schönberg, D., 2020. Stress in the tropics? Impact of a Latitudinal Seawater $\Delta^{18}O$ Gradient on Middle Jurassic temperature reconstructions at low latitudes. *Geology*, 48(12), 1210–1215. https://doi.org/10.1130/G47824.1.

Barclay, R.S., Wing, S.L., 2016. Improving the *Ginkgo* CO_2 barometer: Implications for the Early Cenozoic atmosphere. *Earth and Planetary Science Letters*, 439, 158–171. https://doi.org/10.1016/j.epsl.2016.01.012.

Beerling, D.J., Royer, D.L., 2002. Fossil plants as indicators of the Phanerozoic Global Carbon Cycle. *Annual Review of Earth and Planetary Sciences*, 30(1), 527–556. https://doi.org/10.1146/annurev.earth.30.091201.141413.

Berner, R.A., 1994. GEOCARB II: A revised model of atmospheric CO_2 over Phanerozoic Time. *American Journal of Science*, 294(1), 56–91. https://doi.org/10.2475/ajs.294.1.56.

Berner, R.A., 2006. GEOCARBSULF: A combined model for Phanerozoic atmospheric O_2 and CO_2. *Geochimica et Cosmochimica Acta*, 70(23), 5653–5664. https://doi.org/10.1016/j.gca.2005.11.032.

Berner, R.A., Kothavala, Z., 2001. GEOCARB III: A revised model of atmospheric CO_2 over Phanerozoic Time. *American Journal of Science*, 301(2), 182–204. https://doi.org/10.2475/ajs.294.1.56.

Bodin, S., Mau, M., Sadki, D., Danisch, J., Nutz, A., Krencker, F.N., Kabiri, L., 2020. Transient and secular changes in Global Carbon Cycling during the Early Bajocian Event: Evidence for Jurassic Cool Climate Episodes. *Global and Planetary Change*, 194, 103287. https://doi.org/10.1016/j.gloplacha.2020.103287.

Boucot, A.J., Chen, X., Scotese, C.R., Morley, R.J., 2013. *Phanerozoic Paleoclimate: An Atlas of Lithologic Indicators of Climate*. SEPM (Society for Sedimentary Geology), Tulsa. https://doi.org/10.2110/SEPMCSP.11.

Carmeille, M., Bourillot, R., Brunet, M.F., Bourillot, R., Brunet, M.F., Pellenard, P., Fürsich, F.T., Schnyder, J., Barrier, E., Blanpied, C., Sidorova, I., 2018. Architecture and sedimentary evolution of thesouthwestern Gissar carbonate platform (Uzbekistan) during the Middle–Late Jurassic. *Marine and Petroleum Geology*, 97, 437–465. https://doi.org/10.1016/j.marpetgeo.2018.07.021.

Cavallina, C., Benvenuti, M., Papini, M., 2025. The Middle Jurassic fluvial record of the Central High Atlas (Guettioua Formation, Morocco): Seasonal rivers in a dynamic palaeogeography. *Journal of Palaeogeography*, 14(4), 100272. https://doi.org/10.1016/j.jop.2025.100272.

Chen, F., Dou, Y.W., Huang, Q.S., 1984. *Jurassic Flora of the Western Hills of Beijing*. Geological Publishing House, Beijing, pp. 1–136 (in Chinese).

Chen, L.Q., Li, C.S., Chaloner, W.G., Beerling, D.J., Sun, Q.G., Collinson, M.E., Mitchell, P.L., 2001. Assessing the potential for the stomatal characters of extant and fossil *Ginkgo* leaves to signal atmospheric CO_2 change. *American Journal of Botany*, 88(7), 1309–1315. https://doi.org/10.2307/3558342.

Dera, G., Brigaud, B., Monna, F., Laffont, R., Pucéat, E., Deconinck, J.F., Pellenard, P., Joachimski, M.M., Durlet, C., 2011. Climatic ups and downs in a disturbed Jurassic world. *Geology*, 39(3), 215–218. https://doi.org/10.1130/G31579.1.

Dera, G., Prunier, J., Smith, P.L., Haggart, J.W., Popov, E., Guzhov, A., Rogov, M., Delsate, D., Thies, D., Cuny, G., Pucéat, E., Charbonnier, G., Bayon, G., 2015. Nd isotopeconstraints on ocean circulation, paleoclimate, and continental drainage during the Jurassic breakup of Pangea. *Gondwana Research*, 27(4), 1599–1615. https://doi.org/10.1016/j.gr.2014.02.006.

Dilcher, D.L., 1974. Approaches to the identification of Angiosperm Leaves. *The Botanical Review*, 40(1), 1–157. https://doi.org/10.1007/BF02860067.

Ding, S.T., Sun, B.N., Wu, J.Y., Li, X.C., 2010. Cuticular composition and carbon isotope characteristics of Jurassic *Phoenicopsis (Phoenicopsis) Angustifolia* Heer from Huating in Gansu Province, China. *Journal of Lanzhou University*, 46, 14–21. https://doi.org/10.1017/S0004972710001772 (in Chinese).

Dong, M., Sun, G., 2011. Middle Jurassic plants from Shaerhu coal field of Xinjiang, China. *Global Geology*, 30(4), 497–507. https://doi.org/10.1631/jzus.B1000197.

Doré, A.G., 1991. The structural foundation and evolution of Mesozoic seaways between Europe and the Arctic Sea. *Palaeogeography, Palaeoclimatology, Palaeoecology*, 87(1–4), 441–492. https://doi.org/10.1016/0031-0182(91)90144-G.

Dromart, G., Garcia, J.P., Picard, S., Atrops, F., Lécuyer, C., Sheppard, S.M.F., 2003. Ice age at the Middle–Late Jurassic transition? *Earth and Planetary Science Letters*, 213(3–4), 205–220. https://doi.org/10.1016/S0012-821X(03)00287-5.

Florin, R., 1936. Die fossilen Ginkgophytenvon Franz–Joseeph–Land nebst Erörterungen ueber Vermeintliche Cordaaitales Mesozoischen Alters, I. Spezieller Teil. *Palaeontographica Abteilung B*, 81, 71–173.

Geng, J.Z., Li, H.K., Zhang, J., Zhou, H.Y., Li, H.M., 2011. Zircon Hf isotope analysis by means of LA–MC–ICP–MS. *Geological Bulletin of China*, 30(10), 1508–1513. https://doi.org/10.1016/j.gr.2011.02.010.

Golonka, J., 2004. Plate tectonic evolution of the southern margin of Eurasia in the Mesozoic and Cenozoic. *Tectonophysics*, 381, 235–273. https://doi.org/10.1016/j.tecto.2002.06.004.

Harris, T.M., 1974. *The Yorkshire Jurassic Flora IV Ginkgoales*. Natural History, British Museum, pp. 2–30.

Holz, M., 2015. Mesozoic paleogeography and paleoclimates — A discussion of the diverse greenhouseand hothouse conditions of an alien world. *Journal of South American Earth Sciences*, 61, 91–107. https://doi.org/10.1016/j.jsames.2015.01.001.

Hou, K.J., Li, Y.H., Tian, Y.R., 2009. *In Situ* U–Pb zircon dating using Laser Ablation Multi Ion Counting ICP–MS. *Mineral Deposit*, 28(4), 481–492. https://doi.org/10.1360/972008-2143.

Hu, D., Hou, L., Zhang, L., Xu, X., 2009. A Pre–Archaeopteryz Troodontid Theropod from China with Long Feathers on the Metatarsus. *Nature*, 461, 640–643. https://doi.org/10.1038/nature08322.

Huang, Y.Y., Liang, H., Shao, L.Y., Yang, B., Spiro, B., Zhou, J.M., Lu, J., Fan, T.G., 2024. Extensive carbon cycle between peatland and vegetation: Insights from high net primary productivity of the Middle Jurassic in northwestern China. *Journal of Palaeogeography*, 13(4), 1016–1028. https://doi.org/10.1016/j.jop.2024.06.006.

Husinec, A., Read, J.F., 2023. Milankovitch record from Middle Jurassic platform supports moderate coolhouse glaciation. *Paleoceanography and Paleoclimatology*, 38(12). https://doi.org/10.1029/2023PA004680.

Jackson, S.E., Pearson, N.J., Griffin, W.L., Simon, E., Belousova, 2004. The Application of Laser Ablation—Inductively Coupled Plasma—Mass Spectrometry (LA—ICP—MS) to *In Situ* U—Pb Zircon Geochronology. *Chemical Geology*, 211, 47—69. https://doi.org/10.1016/j.chemgeo.2004.06.017.

Jenkyns, H.C., Jones, C.E., Gröcke, D.R., Hesselbo, S.P., Parkinson, D.N., 2002. Chemostratigraphy of the Jurassic system: Applications, limitations and implications for palaeoceanography. *Journal of the Geological Society*(4), 351. https://doi.org/10.1144/0016-764901-130, 378.159.

Johnson, E.A., Liu, S., Zhang, Y., 1989. Depositional environments and tectonic controls on the coal-bearing Lower to Middle Jurassic Yan'an Formation, southern Ordos Basin, China. *Geology*, 17(12), 1123—1126. https://doi.org/10.1130/0091-7613(1989)0172.3.CO;2.

Judd, E.J., Tierney, J.E., Lunt, D.J., Montañez, I.P., Huber, B.T., Wing, S.L., Valdes, P.J., 2024. A 485—Million—Year History of Earth's Surface Temperature. *Science*, 385, 1316. https://doi.org/10.1126/science.adk3705.

Korte, C., Hesselbo, S.P., Ullmann, C.V., Dietl, G., Ruhl, M., Schweigert, G., Thibault, N., 2015. Jurassic climate mode governed by ocean gateway. *Nature Communications*, 6(1), 10015. https://doi.org/10.1038/ncomms10015.

Korte, C., Hesselbo, S.P., 2011. Shallow marine carbon and oxygen isotope and elemental records indicate icehouse—greenhouse cycles during the Early Jurassic. *Paleoceanography*, 26. https://doi.org/10.1029/2011pa002160. PA4219.

Koschek, G., 1993. Origin and significance of the SEM Cathodoluminescence from zircon. *Journal of Microscopy*, 171(3), 223—232. https://doi.org/10.1111/j.1365-2818.1993.tb03379.x.

Kostina, E.I., Herman, A.B., 2013. Middle Jurassic floras of Mongolia: Composition, age, and phytogeographic position. *Review of Palaeobotany and Palynology*, 193, 82—98. https://doi.org/10.1134/S0031030116120108.

Krassilov, V.A., 1972. *The Mesozoic Flora of the Bureja River (Ginkgoales and Czekanowskiales)*. Nauka, Moscow, p. 115 (in Russian).

Labails, C., Olivet, J.L., Aslanian, D., Roest, W.R., 2010. An alternative early opening scenario for the Central Atlantic Ocean. *Earth and Planetary Science Letters*, 297(3), 355—368. https://doi.org/10.1016/j.epsl.2010.06.024.

Lenton, T.M., Daines, S.J., Mills, B.J., 2017. COPSE Reloaded: An Improved Model of Biogeochemical Cycling Over Phanerozoic Time. *Earth-Science Reviews*, 178, 1—28. https://doi.org/10.1016/j.earscirev.2017.12.004.

Li, J., Huang, C.M., Yang, G.L., Pan, Y.Y., Wen, X.Y., 2022. Middle Jurassic climate oscillations from paleosol records of the Sichuan Basin, SW China. *Journal of Palaeogeography*, 11(1), 97—122. https://doi.org/10.1016/j.jop.2022.01.003.

Li, R.S., D'Alba, L., Debruyn, G., Dobson, J.L., Zhou, C.F., Clarke, J.A., Vinther, J., Li, Q.G., Shawkey, M.D., 2025. Mesozoic Mammaliaforms illuminate the origins of pelage coloration. *Science*, 387(6739), 1193—1198. https://doi.org/10.1126/science.ads9734.

Li, X.B., Zhang, Y., Tong, Y.B., 2021. Preliminary analysis of paleogeography and paleoenvironment during the Jurassic—Cretaceous tectonic transition period in the eastern segment of Yanliao. *Earth Science Frontiers*, 28(2), 391—411. https://doi.org/10.13745/j.esf.sf.2020.6.29.

Li, P.J., He, L.L., Wu, X.W., Mei, S.W., Li, B.Y., 1988. Early and Middle Jurassic Strata and Flora in the Northeastern Margin of the Qaidam Basin, Qinghai. Nanjing University Press, Nanjing, pp. 1—231 (in Chinese).

Li, Y.F., Zhang, C.L., Liang, F., Tan, X., Gong, F.H., Sun, C.L., Li, T., Na, Y.L., 2024. New material of *Coniopteris simplex* from the Middle Jurassic of the Ordos Basin, Inner Mongolia, China and implications on its spatio-temporal distribution and paleogeography. *Journal of Palaeogeography*, 13(2), 199—211. https://doi.org/10.1016/j.jop.2024.03.001.

Liang, F., Tian, N., Sun, W., Wu, Q., Liu, B., Wang, H., 2021. Epidermal features of the floating leaves of *Quereuxia Angulata* (Newberry) Krištofovič, an Aquatic Angiosperm from the Upper Cretaceous of Northeast China. *Cretaceous Research*, 125, 104835. https://doi.org/10.1016/j.cretres.2021.104835.

Liu, Y., Hu, Z., Gao, S., Günther, D., Xu, J., Gao, C., Chen, H., 2008. *In Situ* analysis of major and trace elements of anhydrous minerals by LA—ICP—MS without applying an internal standard. *Chemical Geology*, 257, 34—43. https://doi.org/10.1016/j.chemgeo.2008.08.004.

Liu, Y., Ying, Q.E., Li, Q.J., Zhou, N., Zhang, C., Zhang, Y.J., Tan, X., Liang, F., 2025. *Ginkgoites Manchurica* from the Lower Cretaceous Shahezi Formation of Liaoning, China, and its palaeoclimate implications. *Palaeoworld*, 34(2), 100876. https://doi.org/10.1016/j.palwor.2024.100876.

Longrich, N.R., Vinther, J., Meng, Q., Li, Q., Russell, A.P., 2012. Primi—Tive Wing Feather Arrangement in Archaeopteryz Litho—Graphica and Anchiornis Huzleyi. *Current Biology*, 22(23), 2262—2267. https://doi.org/10.1016/j.cub.2012.09.052.

Ludwig, K.R., 2003. *Isoplot 3.00: A Geochronological Toolkit for Microsoft Excel*, *Berkeley Geochronology Center*. Special Publications, Berkeley, CA. No. 4a.

MacLennan, S.A., Sha, J., Olsen, P.E., Kinney, S.T., Chang, C., Fang, Y., Liu, J., Slibeck, B.B., Chen, E., Schoene, B., 2024. Extremely rapid, yet noncatastrophic, preservation of the flattened—feathered and 3D dinosaurs of the Early Cretaceous of China. *Proceedings of the National Academy of Sciences*, 121(47), e2322875121. https://doi.org/10.1073/pnas.2322875121.

Martínez, C., Gandolfo, M.A., Cúneo, N.R., 2018. Angiosperm leaves and cuticles from the uppermost Cretaceous of Patagonia, biogeographic implications and atmospheric paleo—CO_2 estimates. *Cretaceous Research, 2018*, 89, 107—118. https://doi.org/10.1016/j.cretres.2018.03.015.

Martini, M., Ortega-Gutiérrez, F., 2018. Tectono-stratigraphic evolution of eastern Mexico during the breakup of Pangea: A review. *Earth-Science Reviews*, 183, 38–55. https://doi.org/10.1016/j.earscirev.2016.06.013.

Maruyama, S., Isozaki, Y., Kimura, G., Terabayashi, M., 1997. Paleogeographic maps of the Japanese Islands: Plate tectonic synthesis from 750 Ma to the present. *Island Arc*, 6(1), 121–142. https://doi.org/10.1111/j.1440-1738.1997.tb00043.x.

McElwain, J.C., Chaloner, W.G., 1995. Stomatal density and index of fossil plants track atmospheric carbon dioxide in the Palaeozoic. *Annals of Botany*, 76, 389–395. https://doi.org/10.1006/anbo.1995.1112.

McElwain, J.C., Chaloner, W.G., 1996. The fossil cuticle as a skeletal record of environmental change. *Palaios*, 11(4), 376–388. https://doi.org/10.2307/3515247.

McElwain, J.C., Steinthorsdottir, M., 2017. Paleoecology, ploidy, paleoatmospheric composition, and developmental biology: A review of the multiple uses of fossil stomata. *Plant Physiology*, 174, 650–664. https://doi.org/10.1104/pp.17.00204.

Mi, J.R., Sun, C.L., Sun, Y.W., Cui, S.S., Ai, Y.L., 1996. Paleoecology of Plants and Coal–Accumulating Environments in the Early–Middle Jurassic of Northern Hebei and Western Liaoning. Geological Publishing House, Beijing, pp. 1–169 (in Chinese).

Müller, R.D., Sdrolias, M., Gaina, C., Steinberger, B., Heine, C., 2008. Long–term sea–level fluctuations driven by ocean basin dynamics. *Science*, 319(5868), 135–1362. https://doi.org/10.1126/science.1151540.

Nunn, E.V., Price, G.D., Hart, M.B., Page, K.N., Leng, M.J., 2009. Isotopic signals from Callovian–Kimmeridgian (Middle–Upper Jurassic) belemnites and bulk organic carbon, Stafrin Bay, Isle of Skye, Scotland. *Journal of the Geological Society*, 166(4), 633–641. https://doi.org/10.1144/0016-76492008-067.

Oh, C., Philippe, M., Kim, K., 2015. *Xenoxylon* synecology and palaeoclimatic implications for the Mesozoic of Eurasia. *Acta Palaeontol Polonica*, 60(1), 245–256. https://doi.org/10.4202/app.2012.0132.

Pálfy, J., Smith, P.L., 2000. Synchrony between Early Jurassic extinction, oceanic anoxic event, and the Karoo–Ferrar flood basalt volcanism. *Geology*, 28(8), 747–750. https://doi.org/10.1130/0091-7613(2000)282.0.CO;2.

Park, J., Royer, D.L., 2011. Geologic constraints on the glacial amplification of Phanerozoic climate sensitivity. *American Journal of Science*, 311(1), 1–26. https://doi.org/10.2475/01.2011.01.

Pellenard, P., Tramoy, R., Pucéat, E., Huret, E., Martinez, M., Bruneau, L., Thierry, J., 2014. Carbon cycle and sea–water palaeotemperature evolution at the Middle–Late Jurassic transition, eastern Paris Basin (France). *Marine and Petroleum Geology*, 53(5), 30–43. https://doi.org/10.1016/j.marpetgeo.2013.07.002.

Philippe, M., Puijalon, S., Suan, G., Mousset, S., Thévenard, F., Mattioli, E., 2017. The palaeolatitudinal distribution of fossil wood genera as a proxy for European Jurassic terrestrial climate. *Palaeogeography, Palaeoclimatology, Palaeoecology*, 466, 373–381. https://doi.org/10.1016/j.palaeo.2016.11.029.

Price, G.D., Heszler, B., Charlton, L.M.T., Cox, J., 2023. A climate perturbation at the Middle–Late Jurassic Transition? Evaluating the isotopic evidence from south–central England. *Palaeogeography, Palaeoclimatology, Palaeoecology*, 628, 111755. https://doi.org/10.1016/j.palaeo.2023.111755.

Price, G.D., Rogov, M.A., 2009. An isotopic appraisal of the Late Jurassic Greenhouse Phase in the Russian Platf orm. *Palaeogeography, Palaeoclimatology, Palaeoecology*, 273(1–2), 41–49. https://doi.org/10.1016/j.palaeo.2008.11.011.

Pu, R.G., Wu, H.Z., 1985. *Mesozoic sporopollen assemblages in western Liaoning and their stratigraphic significance*. Geological Publishing House, Beijing, pp. 121–212 (in Chinese with English abstract).

Retallack, G.J., 2001. A 300–million–year record of atmospheric carbon dioxide from fossil plant cuticles. *Nature*, 411(6835), 287–290. https://doi.org/10.1038/35077041.

Royer, D.L., 2003. Estimating latest Cretaceous and Tertiary atmospheric CO_2 from stomatal indices. *Geological Society of America Special Papers*, 369, 79–93. https://doi.org/10.1130/0-8137-2369-8.79.

Scotese, C.R., Song, H.J., Mills, B.J.W., van der Meer, D.G., 2021. Phanerozoic paleotemperatures: The Earth's changing climate during the last 540 million years. *Earth-Science Reviews*, 215, 103503. https://doi.org/10.1016/j.earscirev.2021.103503.

Scott, R.A., Turton, M.A.K., 2001. Mesozoic tectonic events in the North Atlantic and Arctic: Stratigraphic response in an adjacent rift–flank basin (Sverdrup Basin, Arctic Canada). *Polarforschung*, 69(1), 73–83, 10013/epic.29830.d001.

Sellwood, B.W., Valdes, P.J., 2008. Jurassic Climates. *Proceedings of the Geologists Association*, 119(1), 5–17. https://doi.org/10.1016/S0016-7878(59)80068-7.

Seton, M., Müller, R.D., Zahirovic, S., Gaina, C., Torsvik, T., Shephard, G., Talsma, A., Gurnis, M., Turner, M., Maus, S., Chandler, M., 2012. Global continental and ocean basin reconstructions since 200 Ma. *Earth-Science Reviews*, 113(3–4), 212–270. https://doi.org/10.1016/j.earscirev.2012.03.002.

Seward, A.C., 1919. *Fossil Plants. A Text–Book for Students of Botany and Geology. Volume IV. Ginkgoales, Coniferales, Gnetales*. Cambridge University Press, Cambridge, p. 543. https://doi.org/10.1017/CBO9780511710834.

Smith, A.G., Smith, D.G., Funnell, B.M., 2004. *Atlas of Mesozoic and Cenozoic coastlines*. Cambridge University Press. https://doi.org/10.1016/0022-0981(94)90096-5.

Steiner, C., Hobson, A., Favre, P., Stampfli, G.M., Hernandez, J., 1998. Mesozoic sequence of Fuerteventura (Canary Islands): Witness of Early Jurassic sea–floor spreading in the central Atlantic. *Geological Society of America Bulletin*, 110, 1304–1317. https://doi.org/10.1130/0016-7606(1998)1102.3.CO;2.

Steinthorsdottir, M., Jardine, P.E., Lomax, B.H., Sallstedt, T., 2022. Key traits of living fossil *Ginkgo biloba* are highly variable but not influenced by climate — Implications for palaeo-pCO_2 reconstructions and climate sensitivity. *Global and Planetary Change*, 211, 103786. https://doi.org/10.1016/j.gloplacha.2022.103786.

Sun, B.N., Xie, S.P., Yan, D.F., Cong, P.Y., 2008. Fossil plant evidence for Early and Middle Jurassic paleoenvironmental changes in Lanzhou Area, Northwest China. *Palaeoworld*, 17(3–4), 215–221. https://doi.org/10.1016/j.palwor.2008.09.002.

Sun, C.L., Li, Y.F., Dilcher, D.L., Wang, H.S., Li, T., Na, Y.L., Wang, A.P., 2015. An introductory report on the biodiversity of Middle Jurassic Phoenicopsis (Czekanowskiales) from the Ordos Basin, China. *Science Bulletin*, 60(21), 1858–1865. https://doi.org/10.1007/s11434-015-0904-y.

Sun, C.L., Tan, X., Dilcher, D.L., Wang, H., Na, Y.L., Li, T., Li, Y.F., 2018. Middle Jurassic Ginkgo Leaves from the Daohugou Area, Inner Mongolia, China and their implication for palaeo–CO_2 reconstruction. *Palaeoworld*, 27(4), 467–481. https://doi.org/10.1016/j.palwor.2018.09.005.

Sun, G., Yang, T., Tan, X., Miao, Y., 2021. Recent advances in the study of the ferns from Middle Jurassic Baiyanghe Flora of Junggar Basin, Xinjiang, China. *Palaeobiodiversity and Palaeoenvironments*, 101(1), 19–24. https://doi.org/10.1007/s12549-020-00472-x.

Svensen, H., Planke, S., Chevallier, L., Malthe, S.A., Corfu, F., Jamtveit, B., 2012. Hydrothermal venting of greenhouse gases triggering Early Jurassic global warming. *Earth and Planetary Science Letters*, 317–318, 196–207. https://doi.org/10.1016/j.epsl.2007.02.013.

Tian, N., Xie, A., Wang, Y., Jiang, Z., Li, L., Yin, Y., Zhu, Z., Wang, J., 2015. New records of Jurassic petrified wood in Jianchang of western Liaoning, China and their palaeoclimate implications. *Science China Earth Sciences*, 58, 2154–2164. https://doi.org/10.1007/s11430-015-5208-1.

Tralau, H., 1968. Evolutionary trends in the genus *Ginkgo*. *Lethaia*, 1, 63–101. https://doi.org/10.1111/j.1502-3931.1968.tb01728.x.

Wang, J., Chen, S.W., Ding, Q.H., 2013. LA–ICP–MS zircon U–Pb dating, geochemical characteristics of clastic rocks from the Middle Jurassic Wanbao Formation in Tuquan Basin, Inner Mongolia, and constraints on the source area. *Geological Bulletin of China*, 32(8), 1224–1235. https://doi.org/10.3969/j.issn.1671-2552.2013.08.008.

Wang, Y.D., Mosbrugger, V., Zhang, H., 2005. Early to Middle Jurassic vegetation and climatic events in the Qaidam Basin, Northwest China. *Palaeogeography, Palaeoclimatology, Palaeoecology*, 224(1–3), 200–216. https://doi.org/10.1016/j.palaeo.2005.03.035.

Watson, J., Lydon, S.J., Harrison, N.A., 1999. Consideration of the genus *Ginkgoites* Seward and a redescription of two species from the Lower Cretaceous of Germany. *Cretaceous Research*, 20(6), 719–734. https://doi.org/10.1006/cres.1999.0178.

Wu, J.Y., Ding, S.T., Li, Q.J., Sun, B.N., Wang, Y.D., 2016. Reconstructing paleoatmospheric CO_2 levels based on fossil Middle Jurassic paleosols and paleoclimate in Sichuan Basin, China *Ginkgoites* from the Upper Triassic and Middle Jurassic in Northwest China. *Paläontologische Zeitschrift*, 90(2), 377–387. https://doi.org/10.1007/s12542-016-0300-1.

Xu, W.L., Wang, F., Pei, F.P., Meng, E., Tang, J., Xu, M.J., Wang, W., 2013. Mesozoic tectonic regimes and regional oreforming backeround in NE China: Constraints from spatial and temporal variations of Mesozoie volcanic rock associations. *Acta Petrologica Sinica*, 29(2), 339–353. CNKI:SUN:YSXB.0.2013-02-002, (in Chinese with English abstract).

Xu, X., Barrett, P.M., 2025. The origin and early evolution of feathers: Implications, uncertainties and future prospects. *Biology Letters*, 21(2), 20240517. https://doi.org/10.1098/rsbl.2024.0517.

Xu, X., Upchurch, P., Mannion, P.D., Barrett, P.M., Regalado-Fernandez, O.R., Mo, J., Ma, J., Liu, H., 2018. A new Middle Jurassic Diplodocoid suggests an earlier dispersal and diversification of Sauropod Dinosaurs. *Nature Communications*, 9(1), 2700. https://doi.org/10.1038/s41467-018-05128-1.

Xu, X., Zhou, Z., Sullivan, C., Wang, Y., Ren, D., 2016. An updated review of the Middle–Late Jurassic Yanliao Biota: Chronology, taphonomy, paleontology and paleoecology. *Acta Geologica Sinica - English Edition*, 90(6), 2229–2243. https://doi.org/10.1111/1755-6724.13033.

Yan, D., Sun, B., Xie, S., Li, X., Wen, W., 2009. Response to paleoatmospheric CO_2 concentration of *Solenites Vimineus* (Phillips) Harris (Ginkgophyta) from the Middle Jurassic of the Yaojie Basin, Gansu Province, China. *Science in China - Series D: Earth Sciences*, 52(12), 2029–2039. https://doi.org/10.1007/S11430-009-0181-1.

Huang D.Y., Yanliao Biota and Yanshan Movement, *Acta Palaeontologica Sinica*, 54 (4), 2015, 501–546, CNKI:-SUN:GSWX.0.2015-04-008, (in Chinese with English abstract).

Yang X.L. and Sun L.W., Early and Middle Jurassic strata in the southern part of the Greater Khingan Range, *Journal of Stratigraphy*, 9 (1), 1985, 10–20

Yu T.J., Late Mesozoic Magmatism and Sedimentary Characteristics in the Tuquan Area, Western Margin of the Songliao Basin, and Their Regional Tectonic Significance, 2022, Ph.D. Thesis, Jilin University; Changchun, doi:10.27162/d.cnki.gjlin.2022.007502, (in Chinese with English abstract).

Zhang, Q.Q., Li, J.G., Huang, D.Y., 2018. Palynological assemblage of the middle–upper Jurassic haifanggou formation in daohugou, Ningcheng, Inner Mongolia, China. *Acta Micropalaeontologica Sinica*, 35(2), 190–199. https://doi.org/10.16087/j.cnki.1000-0674.2018.02.007.

Zhang, C., Quan, J.Y., Zhang, Y.J., Liu, Z.H., Li, W., Wang, Y., Qian, C., Zhang, L., Ge, J.T., 2020. Late Mesozoic tectonic evolution of the southern Great Xing'an Range, NE China: evidence from whole-rock geochemistry, and zircon UPb ages and Hf isotopes from volcanic rocks. *Lithos*, 362, 105409. https://doi.org/10.1016/j.lithos.2020.105409.

Zhang, Y.J., Yang, Y.J., Liang, F., Wu, X.W., Zhang, C., Fu, J.Y., Wang, Y., Zhang, Q., Liu, M., Ding, Q.H., Zhang, D.J., 2021. The Middle Jurassic palynoflora and its implication for paleoclimate in the western margin of Longjiang Basin. *Geological Bulletin of China*, 40(6), 905–919. https://doi.org/10.12097/gbc.dztb-40-6-905.

Zhang, D.J., Zhang, J., Zheng, Y.J., Chen, S.W., Su, F., Huang, X., Zhang, H.H., 2019. Preliminary study on the Middle Jurassic flora in the southern part of Tuquan Basin, Inner Mongolia. *Geology and Resources*, 28(1), 7–12. https://doi.org/10.13686/j.cnki.dzyzy.2019.01.002.

Zhang, Y., Tian, N., Liang, F., Zhang, C., Li, W., Lou, R., Ma, Y., Du, J., 2021. New Records of Petrified Wood from the Middle Jurassic in Ar Horgin Banner, Lnner Mongolia. *Acta Gieologica Sinica (English Edition)*, 95(2), 684–686. https://doi.org/10.1111/1755-6724.14668.

Zhang, Y., Wu, X., Zhang, C., Guo, W., Yang, Y., Sun, G., 2018. New Evidences for Dating of the Middle Jurasie Wanbao Formation in the Longjiang Basin, Western Margin of Heilongiang Province. *Earth Science Frontiers*, 25(1), 182–196. https://doi.org/10.13745/j.esf.yx.2017-5-22.

Zhou, C.F., Bhullar, B.A.S., Neander, A.I., Martin, T., Luo, Z.X., 2019. New Jurassic Mammaliaform Sheds Light on Early Evolution of Mammal–Like Hyoid Bones. *Science*, 365(6450), 276–279. https://doi.org/10.1126/science.aau9345.

Zhou, N., Wang, Y., Ya, L., Porter, A.S., Kürschner, W.M., Li, L., Lu, N., McElwain, J.C., 2020. An Inter–Comparison Study of Three Stomatal–Proxy Methods for CO_2 Reconstruction Applied to Early Jurassic Ginkgoales Plants. *Palaeogeography, Palaeoclimatology, Palaeoecology*, 542, 109547. https://doi.org/10.1016/j.palaeo.2019.109547.

Zhou, Z.Y., Yang, X.J., Wu, X.W., 2020. *Palaeobotanica Sinica. Ginkgophytes*. Science Press, Beijing, pp. 1–178. https://doi.org/10.3969/j.issn.0001-6616.2020.03.011 (in Chinese, with English abstract).

Ziegler, P.A., 1988. Evolution of the Arctic–North Atlantic and the Western Tethys. *AAPG Memoir*, 43, 1–198. https://doi.org/10.1016/0191-8141(89)90060-6.

Zou, Z.Y., Ma, Q., Xu, Y.G., Liu, L., Xia, X.P., Yang, C.M., 2024. Stratigraphic and U–Pb zircon age constraints on the timing of the Yanliao Biota in Northern China. *Geological Society of America Bulletin*, 136(11–12), 4936–4946. https://doi.org/10.1130/B37497.1.

Appendix A. Supplementary data

Supplementary data to this article can be found online at https://doi.org/10.1016/j.jop.2026.100351.

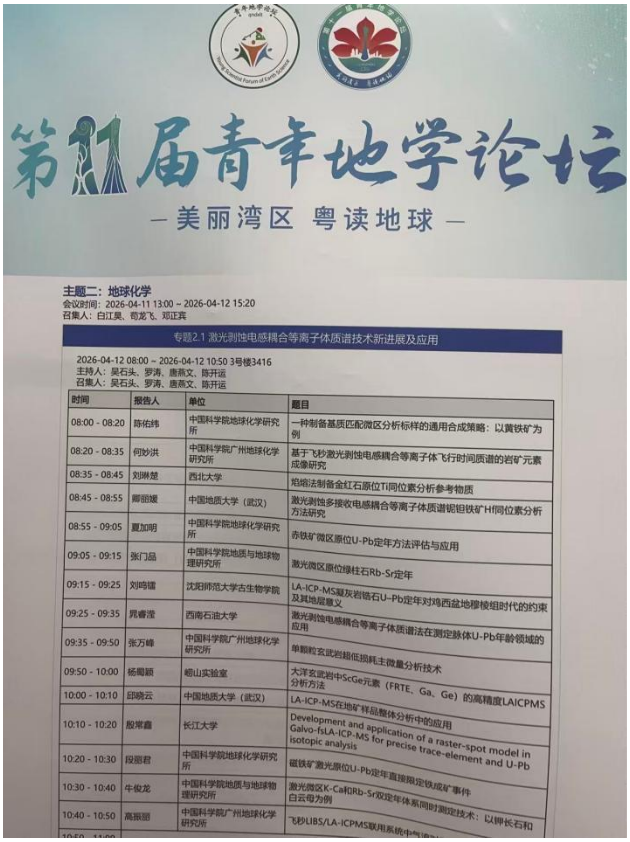

合同编号：2025110640-JH4/4800

辽宁省科学技术计划项目
任务合同书

计划类别：辽宁省科技计划联合计划（自然科学基金-面上项目）

项目名称：玄武岩储层矿物组成对岩石脆性及裂缝发育定量研究

项目编号：2025-MSLH-691

联合单位（甲方）：中国地质调查局沈阳地质调查中心

项目承担单位（乙方）：沈阳师范大学

项目负责人：冯玉辉

合同起止时间：2025-11-01 至 2027-10-31

辽宁省科学技术厅制

3. 主要成员信息

序号	姓名	性别	出生年月	国籍	证件类型	证件号码	统一社会信用代码	所在单位	职称	研究方向	分工
1	冯玉辉	男	1987-08-14	中国	身份证	210203198708145295	12210000463004294L	沈阳师范大学	副高级	油气地质与地球物理	储层分析
2	杜继宇	男	1988-08-15	中国	身份证	370704198808151877	12100000410580554P	中国地质调查局沈阳地质调查中心(东北地质科技创新中心)	副高级	岩石学	矿物识别与鉴定
3	刘鸣镭	男	2002-06-18	中国	身份证	210105200206183758	12210000463004294L	沈阳师范大学	其他	化石能源	数据分析
4	刘畅	女	2001-01-26	中国	身份证	230204200101262129	12210000463004294L	沈阳师范大学	其他	化石能源	数据分析
5	卢镝	女	2005-06-19	中国	身份证	210422200506191525	12210000463004294L	沈阳师范大学	其他	化石能源	数据处理
6	张鹏鸽	女	2000-05-06	中国	身份证	410522200005069364	12210000463004294L	沈阳师范大学	其他	化石能源	数据处理

辽 宁 省 教 育 厅

关于公布2025年度高校基本科研项目立项结果的通知

省内相关高校:

根据辽宁省教育厅《关于发布2025年度高校基本科研项目申报指引的通知》(辽教通〔2025〕186号)要求，经项目依托高校组织专家评审、省教育厅审核，现将立项结果公布如下:

一、全省高校共立项2569项(人文社科类项目1025项、自然科学类项目1544项)，其中，自主选题项目1972项、科研平台建设项目149项、科技创新团队项目191项、创新发展项目257项。

二、各高校要按照《辽宁省高等学校基本科研项目暂行管理办法(试行)》(辽教办发〔2021〕28号)有关规定，加强项目监督与管理，自主开展基本科研项目绩效考核评价，自主确定结题标准，组织结题验收，并报教育厅备案。省属公办本科高校要按照《关于加强基本科研项目管理的通知》有关要求，严格自主管理，严格预算执行，严守财经纪律，加强绩效管理。

三、各高校于12月15日前向省教育厅报送基本科研项目年度

绩效报告。省教育厅将强化评价结果运用，将绩效评价结果作为项目调整、后续支持的重要依据。

附件：2025年度辽宁省教育厅高校基本科研项目立项名单(分发)

辽宁省教育厅
2025年8月29日

序号	状态标志	项目编号	项目名称	负责人	二级单位	所属年度	项目起止时间	总经费（万	人文/自然	项目类别
57	教育厅审核通过	LJ212510166008	辽宁本溪关门山北部早白垩世花岗岩成因及构造背景	白树崇	(018)古生物学院	2025	2025-07至2027-07	3.00	自然科学类	自主选题项目
58	教育厅审核通过	LJ212510166009	FeOOH-富缺陷镍基硫化物的导向构筑及电催化性能研究	毋妍妍	(014)物理科学与技术学院	2025	2025-07至2027-07	3.00	自然科学类	自主选题项目
59	教育厅审核通过	LJ212510166010	面向高速网络的实时细粒度流量测量研究	卜青菲	(020)软件学院	2025	2025-07至2027-07	3.00	自然科学类	自主选题项目
60	教育厅审核通过	LJ212510166011	黑龙江嘉荫K-Pg界线火山事件地球化学示踪与源区识别	冯玉辉	(018)古生物学院	2025	2025-07至2027-07	3.00	自然科学类	自主选题项目

二、项目组成人员情况（含主持人）

姓名	性别	出生年月	专业技术职务	一级学科	二级单位	课题分工	本人签名
冯玉辉	男	1987.8	副教授	地质学	古生物学院	地化分析	冯玉辉
刘畅	女	2001.1	研究生	生物学	古生物学院	岩石鉴定	刘畅
刘鸣镭	男	2002.6	研究生	生物学	古生物学院	数据处理	刘鸣镭
卢镝	女	2005.6	研究生	生物学	古生物学院	数据处理	卢镝
张鹏鸽	女	2000.5	研究生	生物学	古生物学院	制图	张鹏鸽

沈阳师范大学文件

沈师大校〔2026〕99号

关于确定2026年度沈阳师范大学研究生科研与实践创新项目立项的通知

学校各单位：

根据《沈阳师范大学研究生科研与实践创新项目管理办法》（沈师大学位〔2025〕20号）文件规定，经单位推荐、专家评审、网上公示，现确定2026年度沈阳师范大学研究生科研与实践创新项目（以下简称"创新项目"）100项（名单见附件），并就有关事宜通知如下：

一、项目管理

创新项目按照《沈阳师范大学研究生科研与实践创新项目管理办法》进行管理。

1.创新项目建设周期为一年，遇特殊情况需延期的不可超过一年。

2.创新项目实行申请人负责制。全面负责项目的整体规划、具体实施、经费使用、成果总结、结题申报等全过程项目建设工作，项目实施过程中不得更换项目负责人。指导教师应积极关注项目的进展情况，做好研究进度和资金使用记录，并提供必要的指导与监督。

3.项目实施过程中，各培养单位应对创新项目加强过程监督，当项目研究计划、主要研究人员、研究时限需要进行重大调整时，须由项目负责人撰写项目调整说明，经指导教师和培养单位同意后，报研究生院备案。

4.学校将组织专家对项目研究状况予以评估，对无故未按计划开展项目研究、自行更改研究等情况，研究生院将视具体情节做出警告、中止或撤消项目处理，并停止经费使用，追回已开支费用。

二、相关要求

1.项目承担单位应为项目顺利完成提供必要保障条件。

2.项目要在接到本通知后召开项目组全体成员会议，制定具体的实施计划。

3.项目要注重突出创新性、实效性，项目组成员要充分发挥优势，相互配合，密切合作，提交高水平、高质量的研究成果。

4.项目承担单位要高度重视创新项目建设过程管理及成果凝练、应用与转化，及时将项目研究阶段成果应用到高层次人才培养工作实践中。

附件：2026年度沈阳师范大学研究生科研与实践创新项目立项名单

沈阳师范大学

2026年6月2日

沈阳师范大学党政办公室　　　　2026年6月2日印发

附件

2026年度沈阳师范大学研究生科研与实践创新项目立项名单

序号	申报单位	项目类别	项目名称	负责人	项目编号
1	马克思主义学院	人文社科类	责任伦理视域下人工智能创新的挑战与协同治理研究	[illegible]	YJSCX20260001
2	马克思主义学院	人文社科类	算法治理背景下新就业形态劳动者的劳动正义保障研究	[illegible]	YJSCX20260002
3	马克思主义学院	人文社科类	乡村全面振兴背景下农民精神生活共同富裕推进路径研究	[illegible]	YJSCX20260003
4	马克思主义学院	人文社科类	数智技术与哲学概念的深度融合：以"实践观"教学为例的三阶六维模型建构	[illegible]	YJSCX20260004
5	马克思主义学院	人文社科类	传承红色薪火，深耕育人沃土——辽宁红色文化资源赋能高校思想政治教育实践研究	[illegible]	YJSCX20260005
6	国际商学院	人文社科类	ESG表现对企业债务融资成本的影响研究——基于绿色金融发展水平的调节效应	[illegible]	YJSCX20260006
7	国际商学院	人文社科类	人工智能赋能我国金融高质量发展的机理与对策研究	[illegible]	YJSCX20260007
8	国际商学院	人文社科类	人工智能协同驱动辽宁传统制造业绿色生产力培育的理论逻辑与路径机制	[illegible]	YJSCX20260008
9	国际商学院	人文社科类	数字贸易对区域经济韧性的影响研究——基于中国30个省份的面板数据	[illegible]	YJSCX20260009
10	法学院	人文社科类	译文《[illegible]》研究	[illegible]	YJSCX20260010
11	法学院	人文社科类	东北地区低空经济协同发展的法治保障研究	[illegible]	YJSCX20260011

74	古生物学院	自然科学类	准噶尔盆地滴南凸起逆断层体系下石炭系火山岩储层裂缝分布规律研究	刘鸣镭	YJSCX20260074
75	古生物学院	自然科学类	内蒙古突泉盆地中侏罗世木内苏铁类植物研究	项苗苗	YJSCX20260075
76	古生物学院	自然科学类	中国东北早白垩世哺育木的发现及其古生态意义	杨筱萌	YJSCX20260076
77	古生物学院	自然科学类	突泉中侏罗统万宝组孢粉植物群及古环境	马洪伟	YJSCX20260077